Electronic Materials Letters, Vol. 4, No. 3 (2008), pp. 113-129

Electron Emission Characteristics of MgO Thin Films Used for ac-PDPs: Part I. Secondary Electron Emission

Yong-Seog Kim, Sang-Hoon Yoon, Seok-Geun Ahn, Cho-Rong Hong, and Heesun Yang*

Department of Materials Science and Engineering, Hongik University, Seoul 121-791, Korea

In this paper, the electron emission characteristics of MgO, being used as a protection and electron emission layer for ac-PDPs, were examined in relation to glow discharge, crystal structure and defects, and the physics of Auger neutralization reaction. Emphasis has been placed on basic physics associated with secondary electron emission mechanisms from MgO subjected to glow discharge environments. Based on these analyses, we extracted major parameters that may affect the yield of the secondary electron emission and discussed possibilities for improving the yield of the emission.

Keywords: MgO, ac-PDPs, secondary electron emission, glow discharge

1. INTRODUCTION

The recent success of plasma display panels (PDPs) originates from the work of Bitzer, Slottow, and Wilson[1] in 1964. The PDP developed in their research was essentially an array of sub-millimeter-scale cylindrical Neon lamps controlled by a matrix of a driving electronic system. Figure 1 shows a schematic illustration of the plasma display appearing in their original patent.[2] The fundamental concept of their invention was to have 20~40-μm-thick glass dielectric layers on an electrode surface and thereby generate a self-regulating and precisely repeatable dielectric barrier discharge (DBD), as in an ozone generator.[3] A glow discharge without the dielectric layer would become intensified with the progress of discharge time and eventually develop arcs. When the electrodes are coated with an insulating glass dielectric layer, the charged species of the glow discharge will be drawn to and stored on the surface, leading to the formation of wall charges. The so-called wall voltage caused by the wall charge would increase with time to counterbalance the applied electric field. If the wall charge stored reaches a critical value, the effective voltage (i.e. the applied voltage minus the wall voltage) would become smaller than the voltage required to sustain the glow discharge. Thus, the glow discharge would ultimately be extinguished. The wall charge at the dielectric layer of each pixel, on the other hand, allows a memory effect, one of the key features of ac-PDPs. This process of discharge ignition followed by extinction occurs less than one μs, resulting in a short glow discharge pulse. This pulsed discharge can be repeated by applying alternating voltage between the electrodes and the ac-PDP was born from their work. Almost all PDP companies have now adopted these operation principles of ac-PDPs.

The use of a glass dielectric layer on the electrode surface was a practical way of achieving uniform glow discharges over millions of discharge cells. In this configuration, the discharge current or intensity is determined by the thickness of the dielectric layer and the discharge at each cell can have similar discharge characteristics as long as the layer thicknesses are similar. However, it was discovered that this type of layer is not suitable for display devices that are operated for an extended period of time. The glass layer was sputtered by energetic ions and its surface structure and chemical compositions were altered with time. This would change the yield of secondary electron emission from the layer and the firing voltage with time. The secondary electrons are defined as electrons emitted by incident charged species and their emission is very sensitive to the surface structure and its chemical compositions. Such a change in firing voltage is insupportable in a display where one sustain voltage is used for millions of pixels. If the cells have different sputtering history, they will have a range of firing voltages, making it impossible to operate the device with one sustaining voltage. In order to prevent such sputtering of the glass dielectric layer, attempts were made to employ thin film materials with superior resistance against sputtering, including oxide ceramics such as MgO, Al_2O_3, TiO_2, etc, on the surface of the dielectric layer.

Among the various oxides that were evaluated, a 500-nm-thick MgO coating by an electron-beam evaporation process was found to be effective against the sputtering of a dielec-

*Corresponding author: hyang@hongik.ac.kr

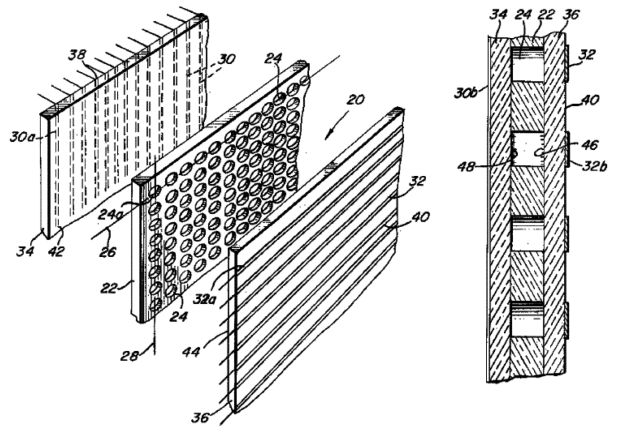

Fig. 1. Drawing from the original plasma display patent.[2]

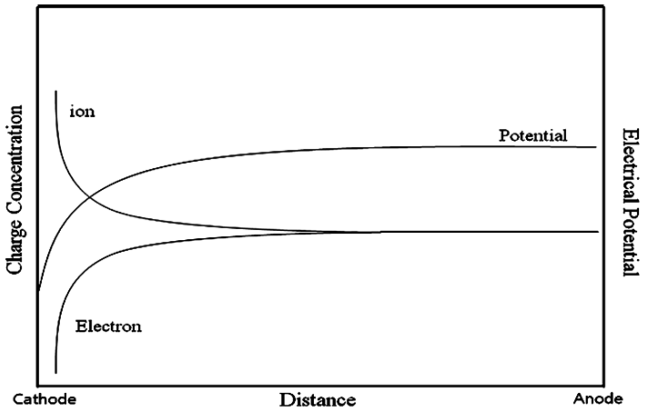

Fig. 2. Schematics of DBD plasma structure.

tric layer and in maintaining the firing voltage at a stable level for the lifetime of device. In addition, the MgO film has a much higher yield of secondary electron emission compared with glass dielectric materials.[4] This high yield is critical in reducing the firing voltage of the glow discharge, since there is a large voltage drop near the cathode surface, as schematically shown in Fig. 2. In the cathode drop region, the positive ions, the mobility of which is approximately 1/1000 that of electrons, are the major current carriers and a high electric field is required to maintain the continuity of current throughout the plasma body. If electron density is increased in this region, the voltage drop will become smaller. The density is determined by the yield of secondary electron emission, and its effect on the firing voltage (V_f) is well described by Paschen's law[5]:

$$V_f = 2.72\frac{g}{h}\ln\left(1+\frac{1}{\gamma}\right) \quad \text{eqn. 1)}$$

where g and h are the constants dependant on the discharge gas composition and γ is the yield of secondary electron emission. As given by eqn. 1), the firing voltage decreases as the yield of the secondary electron emission increases. Another beneficial influence of increased yield is

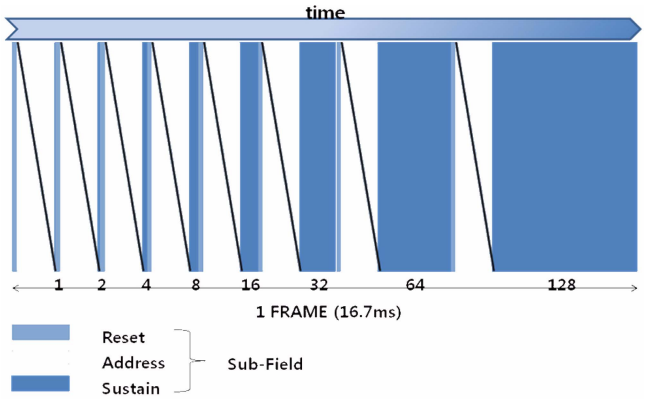

Fig. 3. Address display separation (ADS) driving method for 256 grey levels. One TV-field is divided into 8 sub-fields, and each sub-field is comprised of reset, address, and sustain periods.

enhanced luminous efficiency of ac-PDPs, since the energy spent on heating ions near the cathode drop zone is reduced.[6] The use of a MgO thin film on the dielectric layer has contributed enormously to the enhancement of device performance. Thus, all of the plasma TVs sold today use a MgO layer on the dielectric layer as a protective layer against sputtering as well as an emission layer for the secondary electrons.

In order for an ac-PDP to be used as a display device, the device must be able to reproduce the grey levels of natural images precisely. The pixels of ac-PDPs developed by Bitzer *et al.*[1] operates either in "ON" or "OFF" states. The pulsed discharge of a pixel emits the same amount of visible lights each time and the brightness level cannot be controlled by modulating the voltage or current of the discharge. To address this problem, a technique referred to as the address display separation (ADS) driving method was introduced by T. Shinoda *et al.*[7] In this scheme, the grey scale is achieved by modulating the number of pulsed discharges in a given TV field (16.7 ms for 60 Hz display). First, a TV field is divided into the number of sub-fields and the number of discharges are assigned as 1, 2, 4, . . . or 128 times (8 sub-fields in this case) for each sub-fields. By combining these sub-fields, various grey levels are achieved (256 levels for the 8-sub-field scheme).

Each sub-field consists of reset, address, and sustain periods. To turn "ON" a pixel in a sub-field, wall charges (wall voltage) are deposited on the surface of MgO by inducing an address discharge in the cell (addressing). The standard configuration of commercial ac-PDPs is the coplanar electrode geometry, as shown in Fig. 4. In this configuration, arrays of parallel sustaining electrodes lie on the front glass plate and address electrodes lie on the rear glass plate orthogonal to the sustaining electrode. The gap, d, between the electrodes is on the order of 100 μm and the gas pressure of a rare gas mixture (generally Ne-Xe or Ne-He-Xe) within the pixels, p is about 500 torr. This structure simplifies the address dis-

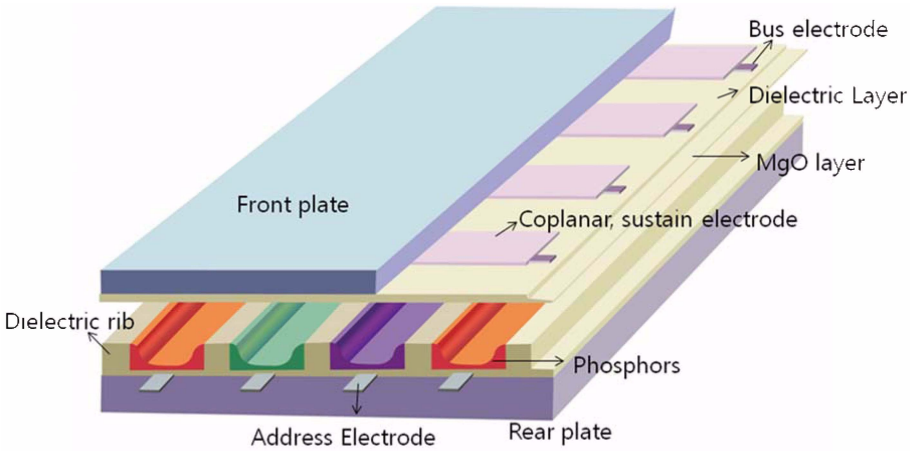

Fig. 4. A schematic illustration of commercial ac-PDP configuration.

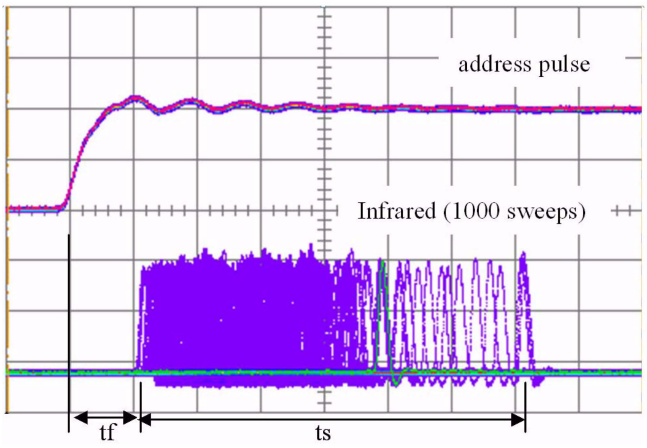

Fig. 5. Statistical variation of address discharge of ac-PDPs.

charge considerably. The addressing discharge is initiated at the intersection of the sustaining and address electrodes by applying appropriate voltages to these electrodes. When a sustaining voltage is applied to all the sustaining electrodes simultaneously (sustaining), only the cells with wall charges will be turned "ON" due to the memory effect noted previously. For this effect, the sustaining voltage applied should be smaller than the firing voltage of the cell, but the sum of the wall voltage and sustaining voltage should be larger than the firing voltage. Under these conditions, only the cells with wall charges (memory of previous discharge event) will be turned ON, while the cells without wall charges remain OFF when the sustaining voltage is applied.

In the ADS driving method, the addressing period consumes a large fraction of the TV frame time, since all the cells must be addressed line by line at each sub-field. For example, if a device has 10 sub-fields (1024 grey levels), the pixel must be addressed 10 times per TV field. The total time necessary to address a display for TV applications is $T_{ad} = N_{SF}(\tau_{reset} + N_{lines} \times \tau_{ad})$, where τ_{ad} is the duration of each address pulse, τ_{reset} the reset time, N_{SF} the number of sub-fields, and N_{lines} the number of lines of the panel. For a Full High Density (FHD) ac-PDP (1920 rows × 1080 lines) with 10 sub-fields, approximately 5 ms is needed for the sustaining period (assuming the sustaining pulse period is 5 μs (i.e., 200 kHz sustaining)). This leaves only 11.7 ms for the reset and addressing operations. In order to have 10 sub-fields, the reset and addressing discharge for each line should be completed in less in than 1.17 μs. The shorter the addressing time, the longer the time that is assigned to the sustaining period for higher grey scales.

When the address voltage is applied between the electrodes, statistical variation in the initiation time of address discharge has been noted to distribute over several μs, as shown in Fig. 5.[8] The scale of abscissa of the figure is 0.5 μs. The data was obtained by detecting the optical output of the address discharge after address voltage pulse application using an infrared sensor. The data of 1000 sweeps were overlapped on an oscilloscope screen. As shown in the figure, the address discharge does not occur immediately after the application of the address voltage pulse. Instead, the time of discharge initiation spreads over a time interval, a so-called a statistical delay. This distribution of the discharge delay has been attributed to variations in the concentration of priming species, especially electrons, within the discharge spaces. All the gas discharges need priming species to initiate the discharge, since the electric field applied between the electrodes is not large enough to ionize the gas atoms in the discharge space. The address discharge will not be initiated until the concentration of the priming species reaches a required value. The priming species, especially the priming electrons, are accelerated by the applied electric field and cause impact ionization of inert discharge gas atoms. The avalanche of electrons by impact ionization leads to ignition of the glow discharge. Thus, the initial concentration of priming species is critical to the statistical variation of the glow discharge initiation.

Several different types of priming species have been

reported to be responsible for the ignition of glow discharge, including space charges and metastables from preceding discharge cycles,[9,10] and exo-electron emissions from MgO.[10-14] The decay time for the space charges of preceding discharge such as electrons and ions reactions has been estimated to be less than a few μs[15] and that for the metastable Xe_2^* dimer through a conversion reaction to Xe^* to be less than 100 μs.[12] However, the conventional ADS driving method of ac-PDPs uses sub-fields of which the time frame is longer than 1 msec. As a result of this short decay time, such priming sources are unreliable for discharge cells that are kept OFF at the preceding subfields.

Exo-electron emission from dielectric materials, on the other hand, are known to have much longer decay time. For example, when an aluminum oxide is irradiated with high energy electrons, delayed emission of electrons from the oxide can be detected even after days of irradiation.[16] This phenomenon is called the Malter effect and is one form of exo-electron emission. In the 1950s, Kramer[17] noted the emission of delayed electrons of low energies from metal oxides after application of mechanical energies (grinding, twisting, stretching, etc.) as well as after exposure to photon and electron radiations. Although different types of energies were delivered onto dielectric materials, electrons of similar energies were emitted from the materials. Assuming that this emission results from exothermic processes, Kramer termed it "exo-electron emission". In an ac-PDP, various forms of discharge energies including UV and visible photon energies, kinetic and potential energies of electrons, and ions irradiating the MgO surface could be the source of exo-electron emission. The emission process is a combination of complex reaction steps and to date there is no commonly accepted theory to explain the kinetics of exo-electron emission.

As discussed above, the electron emission from MgO thin film, whether secondary electron emission or exo-electron emission, is crucial to the performance of ac-PDPs. In this paper, we describe the basic physical mechanisms involved with the electron emissions from MgO film. In part I of this paper, we describe the mechanisms of secondary electron emission and in part II, the mechanisms of exo-electron emission. In addition, trends in recent research toward better electron emission properties are described in each section.

2. MECHANISMS OF SECONDARY ELECTRON EMISSION

2.1. Fundamentals of secondary electron emission

Since T. A. Edison discovered what is now known as as the *Edison effect* in 1883, electron emission phenomena from solid materials have attracted much attention. In his famous light bulb experiment, he detected electric currents between a positively biased electrode and the filament of the bulb. Since the electrodes were separated by the vacuum of the bulb, the detection was attributed to the emission of electrons from the filament followed by attraction to the positively biased electrode. Later, in 1899, J. J. Thomson demonstrated that the *Edison effect* is caused by thermal electrons.[18] The electrons in the red-hot filaments are heated such that a fraction of the electrons acquires enough energy to overcome the potential energy barrier (work function) and escapes from the solid. The thermal energy is used to overcome the potential energy barrier of the solid for the electrons. In 1905, Einstein published a report on the photoelectric effect.[19] In this phenomenon, electrons are excited by photon energy to overcome the potential energy barrier and escape from the solid.

Similar to these electron emission phenomena, electrons may be excited above the potential barrier of a solid by accelerated charged species such as ions and electrons incident on the solid, and then escape from the solid. The electrons emitted by this process are termed secondary electrons. The energies imparted to the electrons by the incident charged species in the form of either kinetic or potential energy help the electrons overcome the potential energy barrier of the solid. The secondary electrons induced by accelerated electrons are the main means of viewing images with a scanning electron microscope (SEM). The number of secondary electrons emitted per each incident particle is called the yield of secondary electron emission.

There are various types of energies available for electron emission from a MgO layer exposed to glow discharges of ac-PDPs. The energies include potential and kinetic energies of charged species such as Ne^+, Xe^+, and He^+ ions as well as electrons, the photon energies of vacuum ultraviolet (VUV) of 147 nm and 173 nm wavelengths and visible lights from phosphors, and energy of metastable species such as Xe^* and Xe_2^* among others. If sufficient energy is imparted to an electron to overcome the potential barrier of MgO, the electrons will be excited to escape from the material. In order to explicate the excitation and escape processes of electrons, basic materials properties of MgO must be introduced.

1) Crystal and band structures of MgO

MgO is a model ionic compound formed between Mg^{2+} cations and O^{2-} anions. Those ions form an interpenetrating face-centered cubic lattice, as shown in Fig. 6. The lattice structure is very symmetric and rigid. Thus, it would be very difficult to form polarons within the lattice when electrons or holes are injected or created within the material. Self-trapped electrons or holes are unstable within MgO.[20] Most of the electrons and/or holes injected to or created within MgO, therefore, must be trapped at donor or acceptor levels, or ejected to outside of the material.

The very strong electro-static attraction between the ions lends the material a very high bond strength, as manifested

in its high melting point (close to 2600°C). This high bond strength makes MgO a potential candidate for the matrix material of radiation detectors.[21] The ionic bonding of the matrix should be strong enough to prevent the formation of defects from irradiation such as γ-rays from nuclear power plants. For that purpose, Chen and his coworkers[21-25] have conducted extensive studies directed toward understanding the basic physical properties of MgO. Recent understanding on MgO defect structures and color centers has benefited from their pioneering research. Similarly, irradiation from the glow discharge of ac-PDPs may also cause damage, and the strong atomic bonding of MgO makes it an ideal material for protection against such damage.

One of the intrinsic characteristics of MgO related with its electron emission properties is the effective mass of electrons within a MgO single crystal. The effective mass of electrons in a MgO single crystal is 0.38,[26] indicating the scattering of electrons within MgO is very minimal, probably likely due to the its regular and symmetric crystal structure. In addition, MgO has a relatively small dielectric constant (~9.8 at 1 MHz).[27] With such a characteristics, the escape distance of excited electrons within MgO is exceptionally large compared with other oxides (~25 nm)[28] and that this increases its the possibility of electron emission.

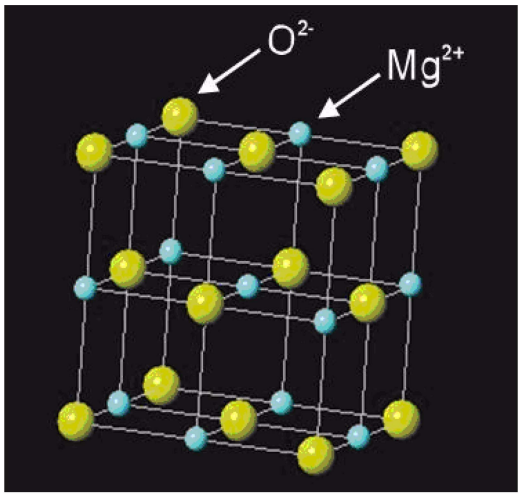

Fig. 6. Crystal structure of MgO. Mg^{2+} and O^{2} ions form interpenetrating facecentered cubic lattices.

The band structure of MgO is also very important for the emission of secondary electrons. The band structure can be understood by assuming energy levels of neutral Mg atoms and O atoms arranged in the facecentered cubic lattice as shown in Fig. 6. With this lattice structure, there will be an upper band of electrons states that are derived from Mg (3s) filled states. There will also be a lower band derived from O (2p) states that are partially occupied. If the electrons from the Mg (3s) orbital are released to find their equilibrium state, all the electrons will drop down to the empty O (2p) states. The conduction band, derived from the Mg (3s) states, will become nominally empty, while the valence band, derived from the O (2p) states, will become nominally filled. This process is illustrated in Fig. 7.

The energy required to excite electrons across the band gap from the valence to conduction band (band gap energy) is related to the energy necessary to transfer the electron from the 2p states of an O^{2} anion to the 3s states of a Mg^{2+} cation. The excitation will neutralize the ions involved and therefore break up the ionic bond. Thus, the band gap energy should be proportional to the bonding energy of the material. Figure 8 illustrates the relationship between the band gap energy and bonding energy of various materials.[29] As noted from the figure, there is a good correlation between the band gap and the bonding energies of the crystals. For bulk MgO, most studies use 7.8 eV as the band gap energy.[30] However, it has been measured or predicted to vary in a range from 6.8 ~ 8.5 eV.[31-32] The insulating characteristic of MgO prohibits precise measurement of the exact value.

Theoretical studies on the energy band structure of MgO have been conducted by numerous researchers. Using the density functional theory (DFT), Avdeev *et al.*[33] calculated

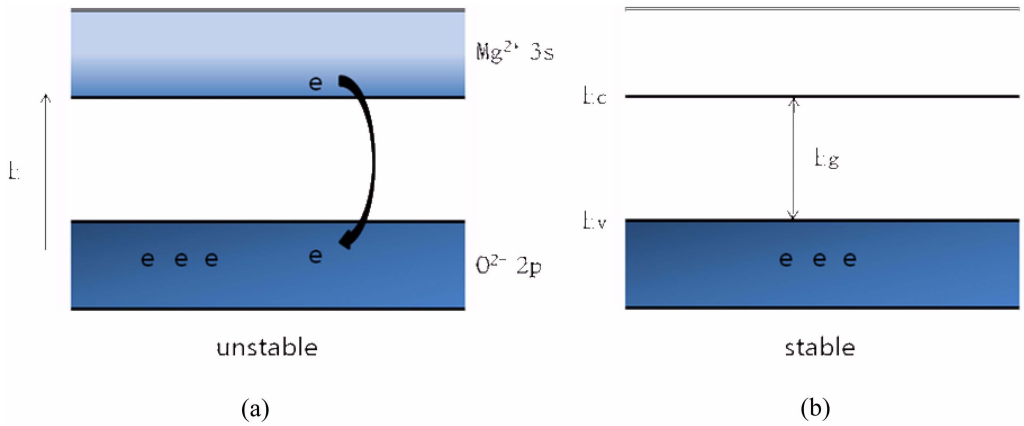

Fig. 7. Development of valence and conduction band of MgO: (a) energy levels of facecentered cubic lattice by neutral Mg and O atoms and (b) band structure after shift of valence electrons from Mg to O.

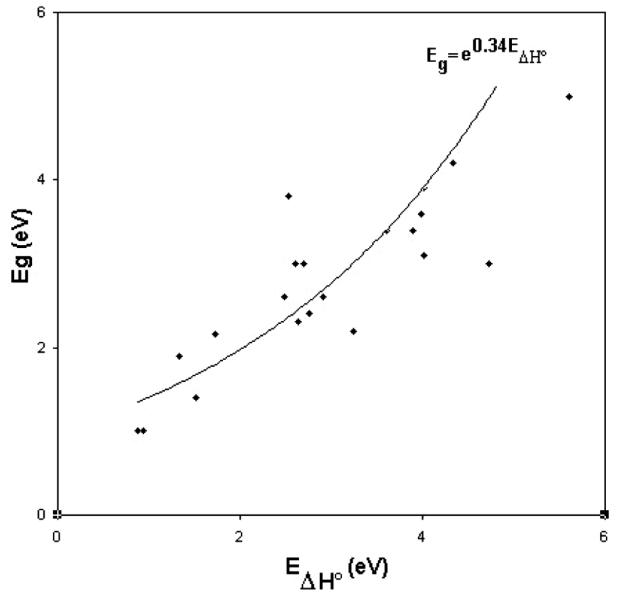

Fig. 8. The band gaps of various materials as a function of the bonding energy of crystals.

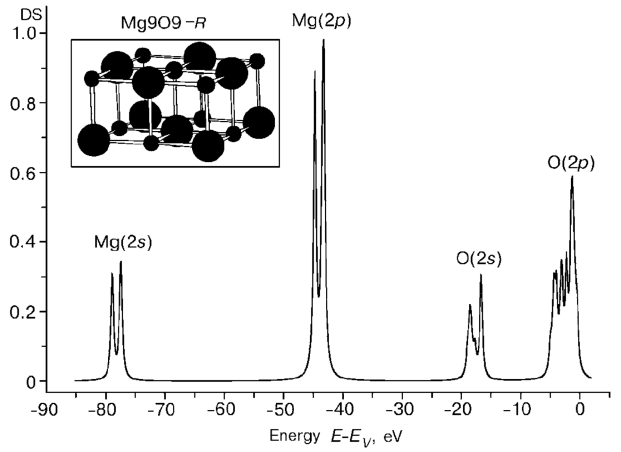

Fig. 9. Density of states of MgO calculated using the density functional theory.[33]

the electronic structure of Mg_9O_9 clusters (Fig. 9). As shown in the figure, the density of state (DOS) comprises relatively narrow bands for Mg (2*s*) and Mg (2*p*) states in an energy range of 40-80 eV, and the valence bands of O (2*s*) and O (2*p*) states in an energy range of 0-20 eV. For the valence band O (2*p*), the band width was 5.4 eV and the energy gap O (2*s* – 2*p*) was 13.5 eV.

Another electronic structure that is important for the emission of electrons is the electron affinity, which corresponds to the width of the conduction band, i.e., the Mg(3*s*) states. Similar to the band gap energy measurement, the electron affinity of MgO has yet to be unequivocally established. While many studies cite a value of 0.85 eV as the affinity,[34] values in a range of 0.85~1.0 eV have been reported by many researchers.[35,36] With small electronic affinity, most of the electrons will be excited over the vacuum level (top of the conduction band) and there will be a relatively small population of electrons excited to the states of the conduction band. This should provide better condition for electron emission from MgO over other materials. If the electron affinity of MgO is zero or negative, most of the electrons excited across the band gap will be emitted into the vacuum. In some cases,[38] a negative electron affinity for MgO has been cited, as in the case of hydrogen terminated diamonds .[39]

As noted above, MgO has various features that make it an ideal material for protection against sputtering of glass dielectric and for electron emission for glow discharge. This discussion is only valid, however, for high purity MgO crystals without any defects. The properties described in the preceding can be altered dramatically by various types of intrinsic and extrinsic defects, as discussed in the following sections.

2) Intrinsic defects of MgO and its energy levels

Intrinsic defects of MgO include the Schottky disorder, electronic defects, and non-stoichiometry. The Schottky disorder could be visualized by displacing the same number of Mg^{2+} cations and O^{2-} anions from inside to its surface. The resulting vacancies at cation and anion sites constitute the Schottky disorders. The defect formation reaction can be represented as follows:

$$\text{null} = V_{Mg}^{''} + V_O^{\circ\circ} \quad \Delta h_f = 7.7 \text{ eV} \quad eqn.\ 2)$$

where $V_{Mg}^{''}$ is the vacancy at the Mg^{2+} cation site and has two negative effective charges. $V_O^{\circ\circ}$ is the vacancy at the O^{2-} anion site and has two positive effective charges. The formation energy (Δh_f) of such disorder is 7.7 eV.[40]

Intrinsic electronic defects are formed by exciting electrons from the valence band to conduction band. The reaction creates free electrons in the conduction band and holes in the valence band. The energy required for such an excitation reaction is the band gap energy of MgO. The reaction can be described as follows:

$$\text{null} = e' + h^{\circ} \quad \Delta h_f = 7.8 \text{ eV} \quad eqn.\ 3)$$

where e' is the free electron concentration at the conduction band and h° is the hole concentration in the valence band.

The defect concentration from the Schottky disorder and electronic defects can be estimated by the following equation.

$$\frac{n}{N} = \exp\left(-\frac{\Delta h_f}{2kT}\right) \quad eqn.\ 4)$$

where *n* is the number of defects and *N* is the number of lattice sites per unit volume. By putting numbers into eqn. 4), the mole fraction of the electronic defects was calculated (Fig. 9). It should be noted that the mole fraction of such

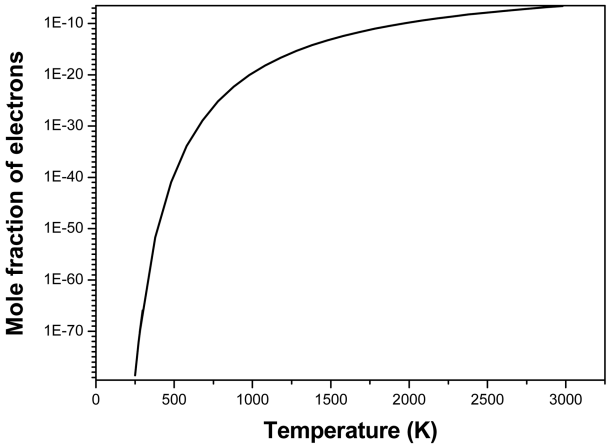

Fig. 9. Mole fraction of electronic defects as a function of temperature.

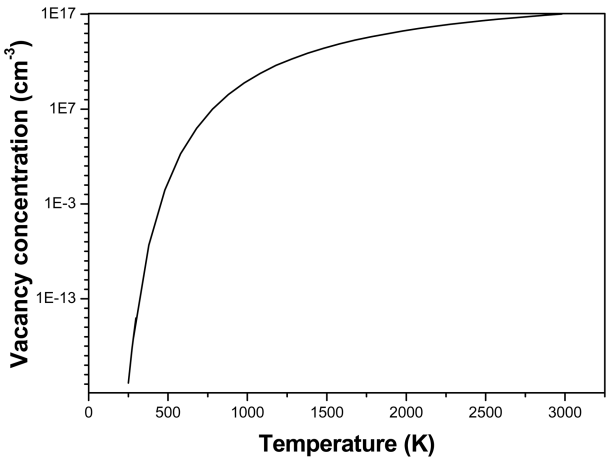

Fig. 10. Equilibrium Mg vacancy concentration in MgO formed under an air atmosphere.

defects is extremely low at ambient temperatures and it would be impossible to measure this defect concentration experimentally. Even at its melting point, MgO has a defect concentration of ~4×10^{-7} (0.4 ppm). This low concentration of intrinsic electronic free carriers makes MgO highly insulating: this may explain the material's capability of excellent wall charge holding characteristics during the period of addressing steps of ac-PDPs. As the formation energy for the Schottky disorders and electronic defects are very similar, the concentration of such Schottky ionic disorders should also be similar, as shown in Fig. 9.

Ceramics exposed to reducing or oxidizing atmospheres are reduced or oxidized according to the following equations of reactions and equilibrium constants:

$$O_O^x=\frac{1}{2}O_2(g)+V_O^{\circ\circ}+2e' \;:\; K_R=n^2[V_O^{\circ\circ}]P_{O_2}^{\frac{1}{2}}=K_R^o\exp\left[-\frac{\Delta g_R}{kT}\right] \quad \textit{eqn.}\ 5)$$

$$\frac{1}{2}O_2(g)=O_O^x+V_{Mg}^{''}+2h^{\circ} \;:\; K_{ox}=\frac{[V_{Mg}^{''}]p^2}{P_{O_2}^{\frac{1}{2}}}=K_{ox}^o\exp\left[-\frac{\Delta g_{ox}}{kT}\right] \quad \textit{eqn.}\ 6)$$

where *n* and *p* are the free electron and hole concentrations and K is the equilibrium constant. The extent of the reaction depends on the free energy of oxidation or reduction, temperature, and partial pressure of oxygen. MgO has a large free energy of oxidation[41] and therefore remains highly stoichiometric. Using experimentally determined values,[26] *eqn.* 6) is rewritten as *eqn.* 7).

$$K_{ox}=\frac{[V_{Mg}^{''}]p^2}{P_{O_2}^{\frac{1}{2}}}=7.2\times10^{63}\exp\left[-\frac{610\ \text{kJ/mole}}{RT}\right]\left(\text{cm}^{-9}MPa^{-\frac{1}{2}}\right) \quad \textit{eqn.}\ 7)$$

Assuming atmospheric oxygen partial pressure (oxidizing atmosphere), the concentration of magnesium vacancies was calculated using *eqn.* 7) (Fig. 10). The actual vacancy concentration at ambient temperature is extremely low, but increases dramatically as the temperature increases. Near the melting point, the magnesium vacancy concentration is 1×10^{17} cm^{-3} (which corresponds to ~1.8 ppm). With further increase in the oxygen partial pressure, the magnesium vacancy concentration will be increased accordingly. These simple calculations show that MgO has very low concentrations of intrinsic defects such as Schottky, electronic, and non-stoichiometric disorders. However, it should be noted that those estimations for defect concentrations are valid only for highly pure MgO formed under thermodynamic equilibrium conditions. The MgO thin films used for ac-PDPs are not formed under equilibrium conditions and such an analysis may only provide a guide line for the estimation of defect concentrations in the films.

3) Extrinsic defects of MgO and its energy levels

The high melting temperature of MgO precludes the use of single crystal growth and purification techniques that are commonly used by scientists working with semiconductors. The universal technique of purification for the oxides is arc fusion. Commercially available MgO materials, therefore, contain a significant amounts of impurities. Table 1 shows typical chemical compositions of commercially available MgO materials with from different sources. It is notable that MgO contains various amounts of metallic impurities, up to thousands of ppm, depending on the source and its form (powder or single crystal). Total impurity content in MgO is several orders of magnitude higher than the intrinsic defect concentration estimated in the preceding section. Therefore, most of the defects observed in MgO may be originated from extrinsic impurities rather than by its intrinsic characteristics.

Table 1. Chemical compositions of commercially available MgO materials (unit: ppm). The letters *S, K,* and *N* denote the source of MgO.[42]

Impurity	Powder(S)	Powder(K)	Single Crystal (N)	Single Crystal (S)
Al	20-50	50	100-200	35
Ca	20	15	300-500	20
Si	15-20	40	10-50	15
Fe	5-20	40	10-50	15
Ni	5	1		2
Mn	1	3	5	1-1
P		7		2
Pb	2-3	<1	<2	<1
S		50		5
Sn	<1			
Cu	<5	<2	<5	<1
Sr		<1	<1	
Ge	1-5			
Mo			<2	
Zn	<20	20	<50	5
Cd, Tl, Pd	<2		<1	
V	<10	<10	30	<2
Mo	<5		<2	
Cr	<10	1	15	<1
As,K	<20	<5		<5
Bi			<1	
Ti	<50	<20	<20	<20
Rb	<50			
Be			<1	
Co	7	<1	<2	
Sb		<1	<5	
Ba		<1	<10	<0.5
Na	20	<20		1
Zr		<1	<20	3

Aliovalent impurities dissolved substitutionally in MgO create point defects according to the following reactions:

$$Li_2O \rightarrow 2Li'_{Mg} + V_O^{\circ\circ} + O_O \quad eqn.\ 8)$$

$$BeO \rightarrow Be_{Mg} + O_O \quad eqn.\ 9)$$

$$Al_2O_3 \rightarrow 2Al_{Mg}^{\circ} + V''_{Mg} + 3O_O \quad eqn.\ 10)$$

$$SiO_2 \rightarrow Si_{Mg}^{\circ\circ} + V''_{Mg} + 2O_O \quad eqn.\ 11)$$

The aliovalent impurities substituting Mg^{2+} cations are generally compensated with ionic defects such as $V_O^{\circ\circ}$ and V''_{Mg}. For example, as shown in *eqn.* 10), Al_2O_3 impurity in MgO creates Al_{Mg}° and V''_{Mg} defects. With such defects, the electrical neutrality of the host lattice is satisfied, since effective charges associated with each defect cancel (compensate) each other precisely. The defects, however, create donor and acceptor levels within the band gap of MgO. Figure 11 shows estimates of the energy levels of such defects.

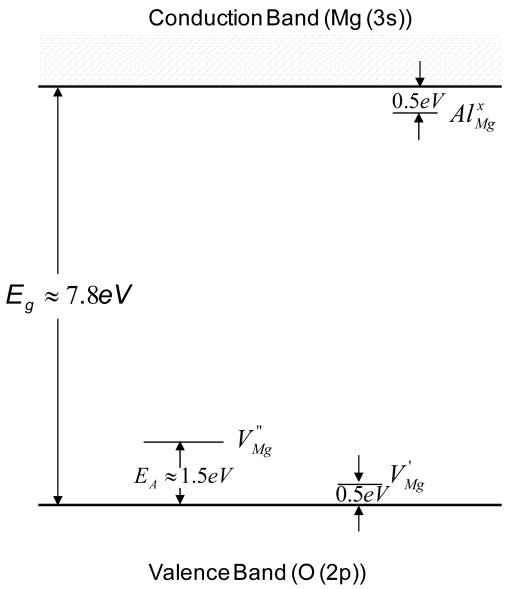

Fig. 11. Energy levels within the band gap of MgO created by Al_2O_3 impurity.

The aluminum impurity creates a donor level by an electron trapping reaction $[Al_{Mg}^{\circ} + e' \rightarrow (Al_{Mg}^{\circ} + e')$ or $Al_{Mg}^{x}]$ roughly 0.5 eV below the conduction band.[43] If Si is the impurity, the excess charge is two ($Si_{Mg}^{\circ\circ}$. Therefore, the trap energy level would be located deeper into the band gap, since the electrostatic attractive force with electrons would be larger. On the other hand, the magnesium vacancy forms an acceptor level by a hole trapping reaction $[V''_{Mg} + h^{\circ} \rightarrow (V''_{Mg} + h^{\circ})$ or $V'_{Mg}]$ approximately 0.5 eV above the valence band. Thus, the extrinsic defects created by impurities could act as trap sites for free electrons or holes, and may influence the electron emission characteristics of MgO. We discuss this aspect in the following section of this paper. One interesting phenomena associated with a magnesium vacancy is that it can trap protons (H^+). Since the magnesium vacancy has negative effective charges, it attracts positively charged species such as proton and holes. If a proton becomes trapped in a magnesium vacancy (some manufacturers form MgO thin film under a hydrogen atmosphere in order to incorporate hydrogen into the film), it creates a donor level ~0.2 eV below the conduction band, the so-called $V_{OH}^{\cdot}$ center.[44] The hole trapping site is transformed to an electron donor site by hydrogen doping.

Using the pseudo-hydrogen model,[45] the donor level (Al_{Mg}^{x}) can be estimated theoretically by the following relationship:

$$E_T = 13.6\left(\frac{m_e^*}{m_e^o}\right)\left(\frac{1}{\varepsilon_r^2}\right)(\text{eV}) \quad \textit{eqn.}\ 12)$$

where m_e^* denotes the electron effective mass in MgO ($m_e^* = 0.38 m_e^o$, m_e^o the electron mass in under vacuum, and ε_r the relative dielectric constant of MgO ($\varepsilon_r = 9.8$). Using these values, the trap level was estimated to be approximately 0.05 eV below the conduction band. The estimated level is very shallow and is significantly different from values reported in the literature.[43] These shallow levels are very difficult to determine experimentally, and therefore, more works are needed to determine the exact locations of such donor or acceptor levels within the band gap.

The oxygen vacancy ($V_O^{\circ\circ}$) in MgO is of significant research interest since it affects the physical appearance of MgO. The oxygen vacancy has two positive effective charges and can serve as a trap site for electrons through electronic compensation reactions as follows:

$$V_O^{\circ\circ} + e' = V_O^{\circ} \quad \textit{eqn.}\ 13)$$

$$V_O^{\circ} + e' = V_O^{x} \quad \textit{eqn.}\ 14)$$

These traps are known as F^+- and F-center, which originate from the German word *Farbzentrum* or color center. The F-center is an oxygen vacancy filled with two electrons (V_O^x) and the F+-center is filled with one electron (V_O°). These centers are often paramagnetic and are studied by electron paramagnetic resonance techniques. These traps tend to emit light in the visible spectrum and MgO, which is usually transparent, becomes colored with the centers. For example, electrons in the F-type centers can be excited to conduction band or electron trap levels. These electrons can recombine with F-types centers to release electromagnetic radiations of 390 nm (3.2 eV) or 540 nm (2.3 eV), as shown in Fig. 12[23] and result in coloration of MgO.

F-type centers could be formed via several pathways, including the addition of alkaline elements, processing under a reducing atmosphere, and ionizing radiation. As shown in eqn. 8), each alkaline element produces one oxygen vacancy. The alkaline elements in commercial MgO are not rich (refer to Table 1), and therefore, most F-type centers are not caused by these impurities. If MgO is prepared under a reducing atmosphere (for example, under Mg vapor at elevated temperatures), a few hundred ppms of magnesium vacancies are created in MgO single crystals.[44]

Finally, other extrinsic defects that may affect the emission of secondary electrons include dislocations, grain boundaries, and surface defects. Dislocations formed during the production of a material can serve as preferential segregation sites for aliovalent impurities as well as sites for precipitations.[46] On the other hand, grain boundaries of crystalline solids are the source and sink of vacancies. In addition, they provide a site for preferential segregation for solute atoms since they have a relatively open structure. Grain boundaries are among the major defects that can be observed with MgO thin films formed by an electron-beam evaporation process. The grain size of the film is on the order of 40 nm and a significant fraction of atoms are located at the boundaries. Merely a small amount of impurities segregated to the boundaries can have a profound effect on the properties of MgO. This is especially critical in the case of MgO, since its grain boundaries are charged by segregation.

With pure MgO, Mg^{2+} ions are segregated more to the grain boundaries than O^{2-} ions, as schematically illustrated in Fig. 13(a), since the formation energy of magnesium vacancies is much smaller than that of oxygen vacancies.[47] Therefore, the grain boundary is charged positively and the excess Mg^{2+} cations can become electron trap sites. However, when Al_2O_3 is added to MgO, it changes the segregation behavior, as shown in Fig. 13(b). In this case, O^{2-} is the element that segregates more to the grain boundaries, and thus the nega-

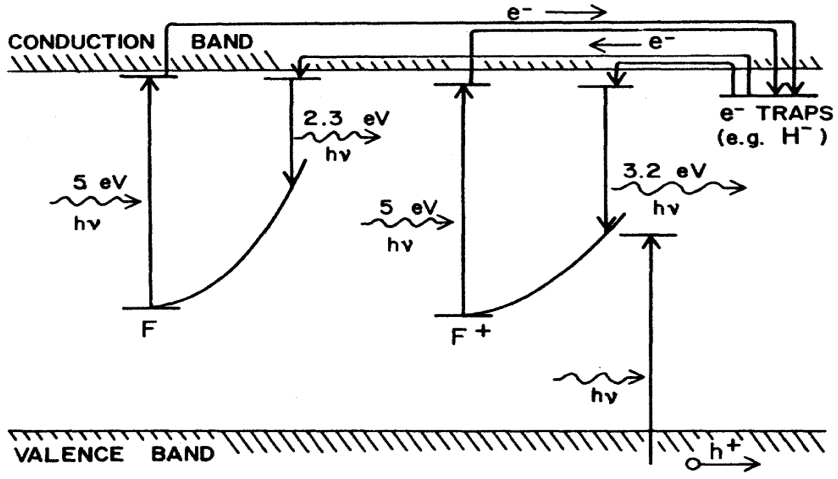

Fig. 12. Energy levels of F-type centers and cathodoluminance emission.[23]

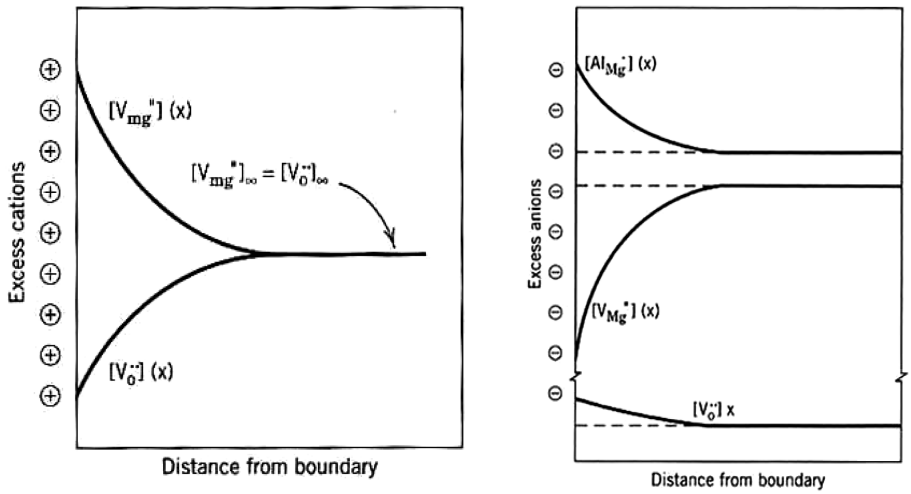

Fig. 13. Grain boundary charging: (a) pure MgO and (b) Al_2O_3 doped MgO.

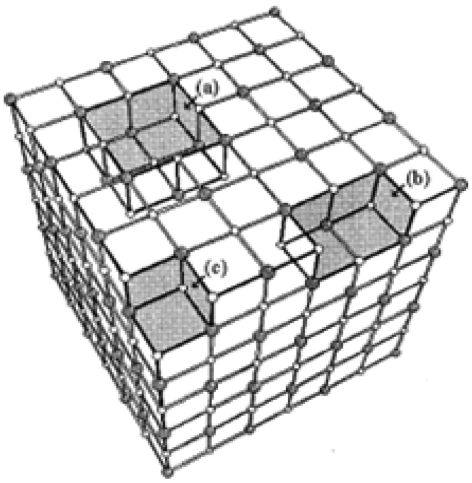

F-Center	Location	Formation E. (eV)
F(6c)	Bulk	9.7
F_s(5c)	Terrace	8.1
F_s(4c)	Step	6.9
F_s(3c)	Corner	5.6

Fig. 14. Surface defects and surface vacancy formation energies at such defects.

tively charged grain boundaries can become hole trap sites. It is apparent that the grain boundaries of MgO may be either electron or hole trap sites depending on the type of major impurities incorporated, but its energy levels may be different from that of the matrix.

The MgO surface may have various types of defects, including steps, kinks, and surface vacancies, as shown in Fig. 14. These defects affect the chemical and physical properties of the surface. For example, a nearly defect-free MgO(1 0 0) single crystal surface is chemically inert towards molecular adsorbates that physisorb only at very low temperature; on the contrary, a polycrystalline surface rich in color centers is highly reactive and promotes the formation of complex radical anions. There is very little direct experimental information on the structure and energetics of these surface defects for MgO. Theoretical estimation showed that the F-type centers can form with much smaller energy at these defects, as shown in the table of Fig. 14.[48] Thus, the surface of MgO should have a much higher concentration of F-type centers and other defects associated with dangling bonds.

In addition, the bonding energy between ions near the surface is lower than the bulk of MgO due to the dangling bonds. This should reduce the band gap energy near the surface. Kramer *et al.*[49] estimated that the band gap could be decreased by more than 1eV compared with that of bulk. Thus, the band gap energy could be less than 6.8 eV near the MgO surface.

2.2. Secondary electron emission via Auger neutralization reaction

1) Energy sources for secondary electron emission

As noted in the previous section, various types of energy

are available for electron emissions from MgO exposed to glow discharges of ac-PDPs: potential and kinetic energies of ions, VUV photon energies, and energy of metastables species. MgO irradiated with photons of sufficient energy may emit electrons by a photo-electric effect, as shown in Fig. 15.[38] Photons abundant in the glow discharges of ac-PDP are VUVs of 147 nm (resonance radiation) and of 173 nm (molecular radiation) wavelength. The photon energy of the radiation corresponds to 8.4 eV and 7.2 eV, respectively. Among the types of radiation, resonance radiation is readily absorbed by other Xe atoms (self-absorption) and the collision cross section with the valence electrons is rather small (1/1000 of ion). Thus, the emission of electrons by this energy source is expected to be rather insignificant. With respect to molecular radiation, its energy is slightly smaller than the band gap energy. Excitation reaction with this photon energy will only be feasible near the surface, where the band gap energy is slightly smaller. This excitation reaction, therefore, has a small interaction volume, making the contribution of this reaction to the yield of secondary electron emission negligible.

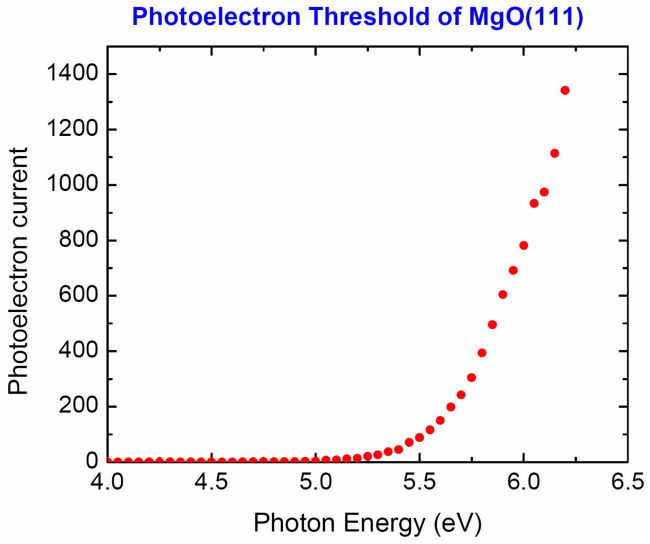

Fig. 15. Photoelectron current from MgO as a function of photon energy.

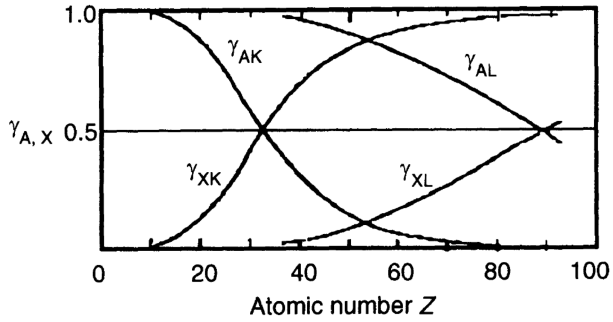

Fig. 16. Emission probability of an Auger electron (A) or photon (X) from the neutralization reaction of ions.

Unlike the photon and metastables energy sources, the positive ions in a glow discharge, such as Ne^+, He^+, and Xe^+, are driven towards the MgO surface by applied voltage. As the ions approach the surface, electrons from MgO tunnel through its surface and react with incident ions to release neutralization energy. The released energy from the reaction can be spent in either ejecting electrons or in generating electromagnetic radiation. This former process of electron emission is called the "Auger Neutralization" mechanism of secondary electron emission. For MgO, which consists of elements of low atomic numbers, there is a much larger possibility of ejecting electrons with the neutralization energy than with electromagnetic photon radiation, as schematically shown in Fig. 16.[50] With elements of low atomic numbers, the Auger electron emission is favored considerably over the photon radiation.

This electron emission process by positive ions (Auger mechanism) is very efficient compared with photon energies (photo-electric effect). In the Auger mechanism, the energy source (ions) is driven towards the MgO surface by the applied field. The photons and metastables move randomly and could be wasted before the reaction occurs at the MgO surface. Thus, most of the ions are used for the Auger neutralization reaction. In addition, the collision cross section for the Auger mechanism is much larger than the photo-electric reaction. Therefore, the Auger neutralization reaction of ions is not wasted as long as the reaction is allowed thermodynamically. This point will be further discussed later in this section. Therefore, it seems that most of the secondary elec-

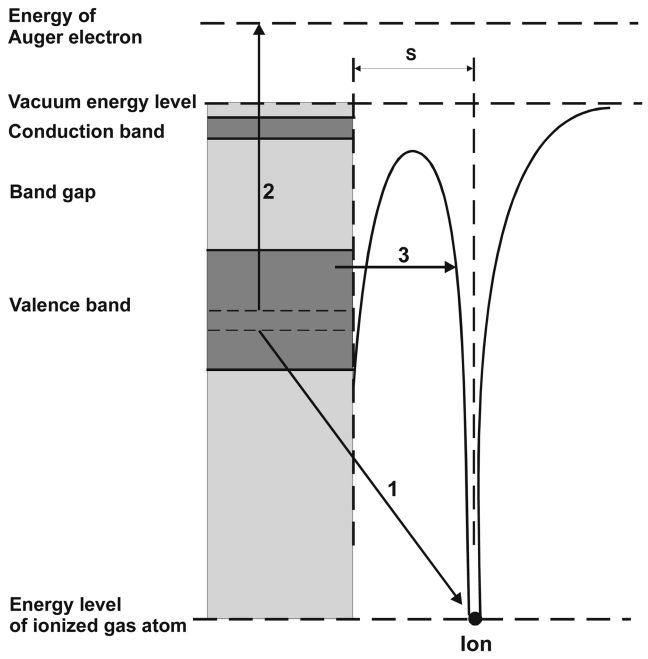

Fig. 17. Secondary electron emission mechanism of Auger neutralization (1 & 2) and resonance neutralization followed by Auger-de-excitation step (3).

trons of glow discharges of ac-PDPs originated through the Auger mechanism.

2) Secondary electrons emission via Auger reactions

The theory of electron emission due to Auger ejection of electrons from diamond-type semiconductor surfaces is well documented in the classical paper by Hagstrum.[51] In his model, the electron emission by the potential energy of low kinetic energy ions is considered. The theory shows that the secondary electron emission is a combination of (a) Auger neutralization and (b) resonance neutralization followed by Auger de-excitation, as illustrated in Fig. 17. With the Auger neutralization mechanism, the energy released from the neutralization reaction (route '1' in the figure) is spent to eject an electron (route '2' in figure). With the resonance neutralization process, the reaction between an incident ion and a tunneled electron forms an excited atom (route '3' in the figure). The energy released upon de-excitation may be used in exciting electrons from its valence band. For this reaction to occur, however, the excited energy level of the gas atom must resonate with electrons in the valence band of MgO. Thus, this resonance neutralization reaction will occur only with the atoms that can satisfy such requirements.

The energy band structure of MgO along with ionic and excited states of the discharge gas are shown in Fig. 18. Among the gas atoms, the resonance neutralization reaction may occur only with Ar ions, since the energy level of the excited state lies within the valence band. In the case of Xe, there might be some possibility of reaction if the band gap energy of the MgO surface is smaller than 7.8 eV. Howerver, such resonance neutralization reactions of Xe ions may not result in extensive emission of electrons, since the number of electrons available for the reaction would be limited to those at the surface. Therefore, the electron emission through the resonance neutralization of Xe^+ ions followed by Auger de-excitation may not play a significant role in the emission of secondary electrons from MgO in ac-PDPs. For the Ne^+ and He^+ ions, the resonance neutralization reaction does not occur, since the excited state levels do not resonate with the

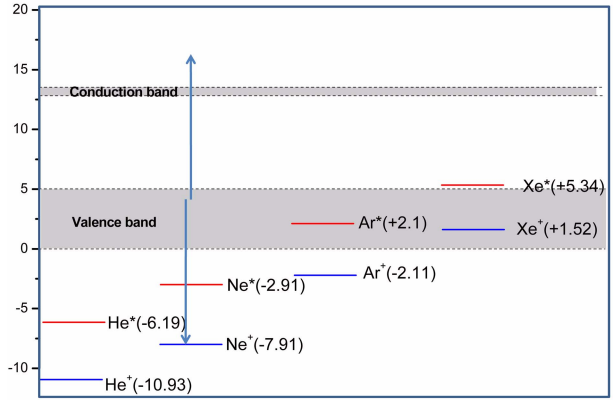

Fig. 18. Energy bands of MgO and levels of discharge gas ions and excited state of atoms.

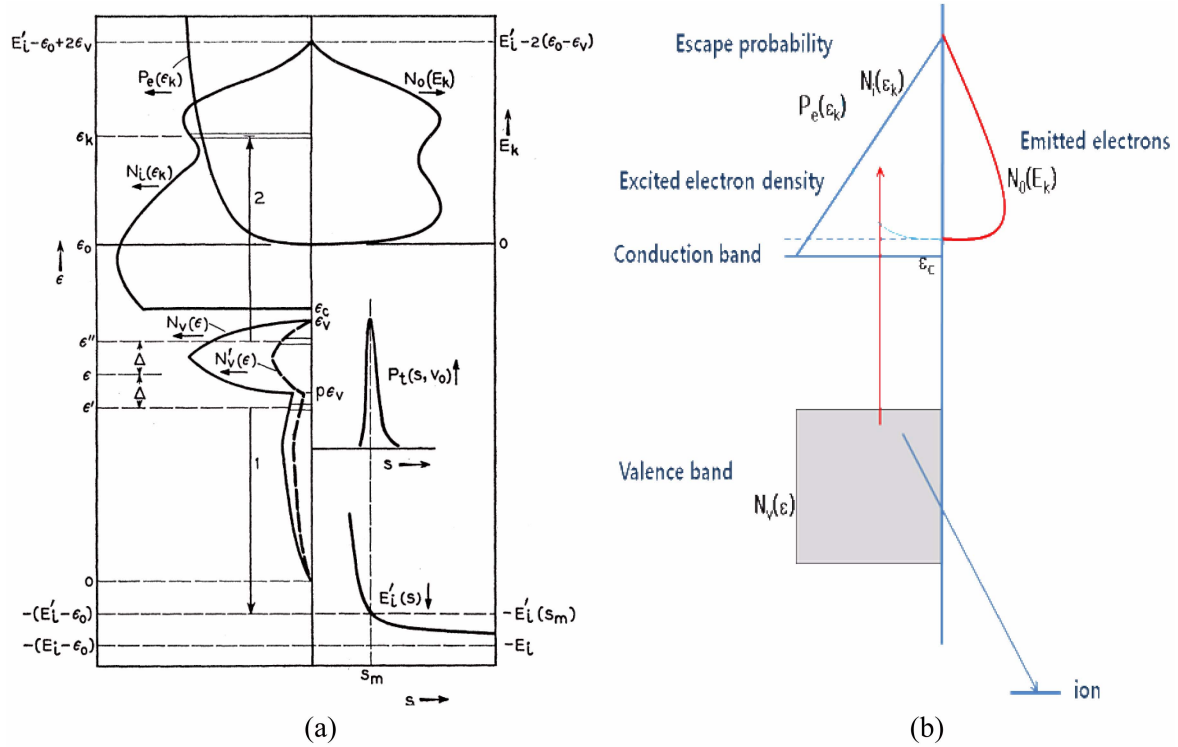

Fig. 19. Reaction steps of secondary electron emission via Auger neutralization process: (a) diamond type semi-conductor and (b) MgO with flat valence band.

electrons in the valence band. With those ions, only the direct neutralization reaction (downward arrow in the figure for Ne^+ ions) can excite the electrons within the valence band to the vacuum level (upward arrow above the top of the conduction band), i.e., the Auger neutralization mechanism.

3) Reaction steps of secondary electron emission via Auger neutralization reaction

Hagstrum[51] theorized the reaction steps of the secondary electron emission process via the Auger neutralization reaction, as illustrated in Fig. 19(a). An approaching ion reacts with an electron that has tunneled through the MgO surface (path 1). For the reaction, the density of state in the valence band is given as the N(curve. Since the electron may have different reaction probability with the ion depending on its orbital configuration, the density of state available for the reaction $N'(\varepsilon)$ is obtained by multiplying the transition probability. However, in the case of MgO, the electrons in the valence band have the same orbital configuration and this adjustment may not be necessary. The energy from the neutralization reaction pumps the electrons from the valence band to the energy levels available above the conduction band. The number of electrons excited to an energy level of $_k$ can be calculated by using a matrix element of the Auger process, which is defined by the following equation:

$$T(\varepsilon) = \int N_v'(\varepsilon-\Delta)N_v'(\varepsilon+\Delta)d\Delta \quad eqn.\ 15)$$

Using eqn. 15), the density of electrons excited is calculated as the curve $N_i(\varepsilon_k)$ of the figure. The excited electrons are free to move within the MgO. During the process, they can be scattered and lose parts of their energy by elastic interaction with phonons, or be trapped by defects, such as those discussed in the previous section. The electrons that reach the surface with energies higher than the vacuum level can escape from the MgO surface. The probability of such excited electrons escapeing from MgO, therefore, is a function of energy as well as the electron trap concentration of MgO. Thus, the probability of escape from MgO must be multiplied to the density of electrons excited in order to obtain the density of electrons emitted ($N_0(\varepsilon_k)$).

Typically, the escape probability is modeled using a parabolic type function of electron energy ($P_e(\varepsilon_k)$), as shown in the figure. After obtaining those functions, the yield of secondary electron emission is obtained from the ratio between the electrons emitted (integrated area of curve $N_0(\varepsilon_k)$) vs. electrons excited (integrated area of curve $N_i(\varepsilon_k)$) :

$$\gamma = \frac{\int_0^\infty N_0(\varepsilon_k)d\varepsilon_k}{\int_{\varepsilon C}^\infty N_i(\varepsilon_k)d\varepsilon} \quad \text{eqn. 16)}$$

From this Auger neutralization model of secondary electron emission from MgO, the parameters that may affect the yield of secondary electron emission can be extracted. The parameters include the band gap energy and electron affinity of MgO, the ionization energy of discharge gas, and the escape probability (defect concentration in MgO).

2.3. Factors Affecting Secondary Electron Emission from MgO due to Auger Effect

Using a modified version of Hagstrum's model for MgO (Fig. 19(b)), the yield of secondary electron emission has been predicted by various researchers and measured experimentally. In this section, the effects of parameters selected above on the yield of secondary electron emission are reviewed.

1) Effects of discharge gases

According to the energy diagram presented in Fig. 18, electrons in the MgO valence band can be excited above the vacuum level by the energy released from the Auger neutralization reaction if the following condition is satisfied:

$$E = E_i^0 - 2(E_G + \chi) > 0 \quad \text{eqn. 17)}$$

where E_i^0 is the ionization energy of gas atoms, E_G is the band gap energy, and χ is the electron affinity of MgO. The energy 'E' in eqn. 17) represents the maximum excess energy of electrons available for escape from MgO. Therefore, for a given MgO energy band structure, the yield of secondary electrons will increase with the ionization energy (E_i^0). If we assume the band gap energy and electron affinity as 7.8 eV and 0.85 eV, the maximum excess energy is negative for Ar, Kr, and Xe. Thus, for these ions, it is not possible to emit secondary electrons via the Auger neutralization process, as shown in Fig. 20.[52]

The experimentally measured yield of secondary electron emission is shown in Fig. 21. As expected, the yield from Xe+ and Kr+ ions is almost negligible in the region of low kinetic energy. This indicates that the Auger neutralization

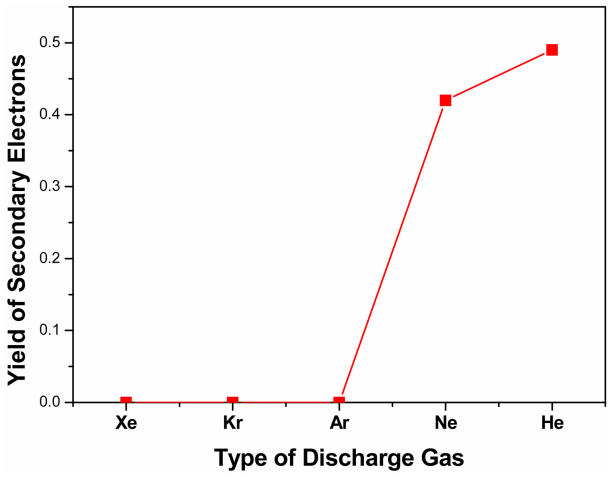

Fig. 20. Effect of discharge gas type on the yield of secondary electron emission.

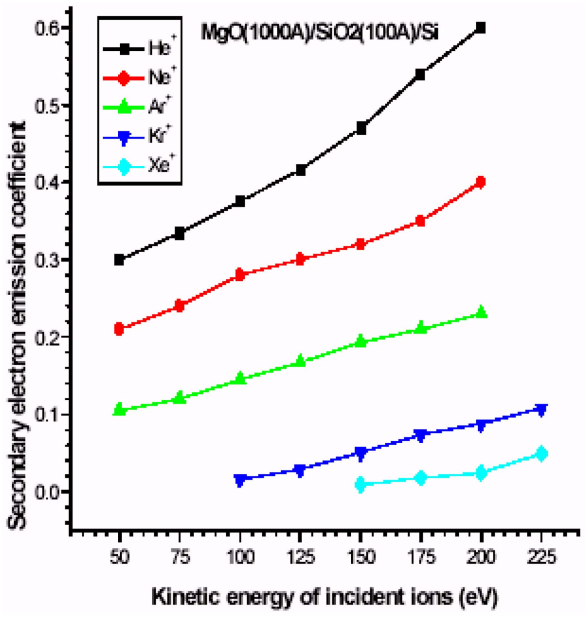

Fig. 21. Effect of discharge gas type on the yield of secondary electron emission measured experimentally.

reaction is the main mechanism of secondary electron emission, and resonance neutralization followed by a de-excitation reaction may not occur, as discussed in the preceding section. For Ar^+ ions, contrary to the zero yield by the Auger neutralization reaction (Fig. 20), experimental data showed a significant yield of secondary electrons (Fig. 21). This difference could be caused either by the emission of secondary electrons by resonance neutralization followed by the de-excitation reaction or by the smaller bandgap of MgO. As shown in Fig. 18, secondary electrons can be emitted by the resonance neutralization process for Ar^+ ions. Therefore, the experimentally measured yield with Ar^+ ions may originate from the resonance neutralization reaction. If the band gap energy is 6.8 eV, as Motoyama *et al.*[53] assumed, instead of 7.8 eV, the Auger neutralization model predicts the yield to be around 0.1, which is similar to the experimentally measured value.

2) Effects of band gap energy and electron affinity

If the band gap energy E_G, and the electron affinity, χ, of MgO in eqn. 17) are decreased for a given ion, the maximum excess energy available for the emission of secondary electrons should increase. Using the same theoretical model as given in Fig. 19(b), the effect of the band gap energy on the yield of secondary electrons from the Auger neutralization reaction with Xe ions was predicted.[52] In this case, the electron affinity was assumed to be 0.85 eV. The secondary electron yield remained zero until the band gap energy was decreased to less than 5.2 eV. At a band gap energy smaller than that value, a slight reduction in band gap energy resulted in a significant increase in the yield. Thus, it would

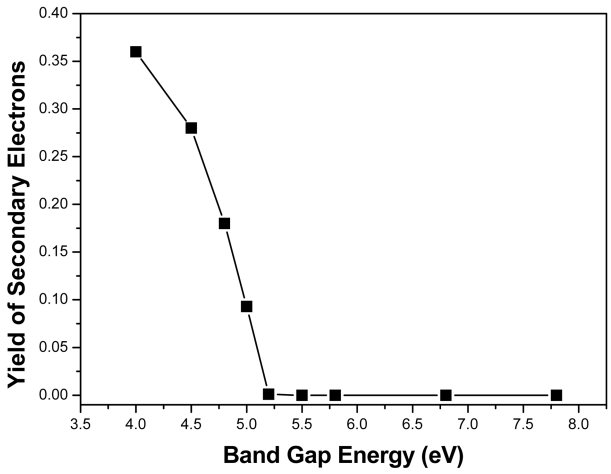

Fig. 22. Effect of band gap energy on the yield of secondary electrons from the Auger neutralization reaction with Xe ions.

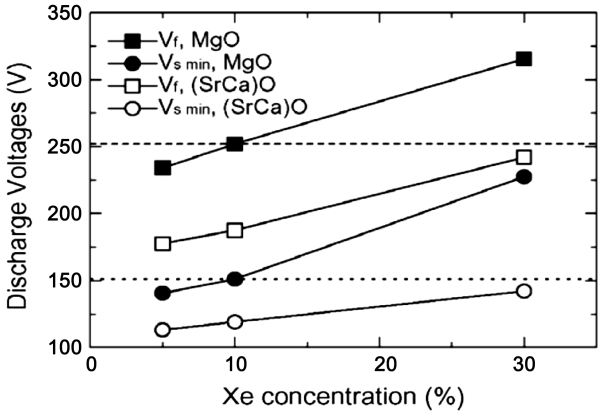

Fig. 23. The firing voltages of test panels with MgO or (SrCa)O.

be desirable to reduce the band gap of MgO in order to yield secondary electrons from the Auger neutralization reaction of Xe^+ ions. Recently, the emission of secondary electrons from Xe^+ ions has become critical as the Xe content in discharge gas is increased in order to enhance the luminance efficiency of ac-PDPs.[54] The secondary electrons emitted from the Auger neutralization reaction of Xe^+ ions are essential for maintaining low firing voltages with discharge gases having high Xe contents.

One of the easiest ways to reduce the band gap energy is to create alloys with other oxides of low band gap energies. For example, CaO, which has a similar band gap structure to MgO, is alloyed with SrO, which has a band gap of 5.4 eV. The electron emission layer with this alloy results in much lower firing voltages compared with pure MgO (Fig. 23). Unfortunately, modification of the band gap energy without affecting the crystal structure and chemical compositions of MgO appears to be impossible. However, we cannot exclude the possibility that other parameters are causing the reduced firing voltage in the case of (SrCa)O compound.

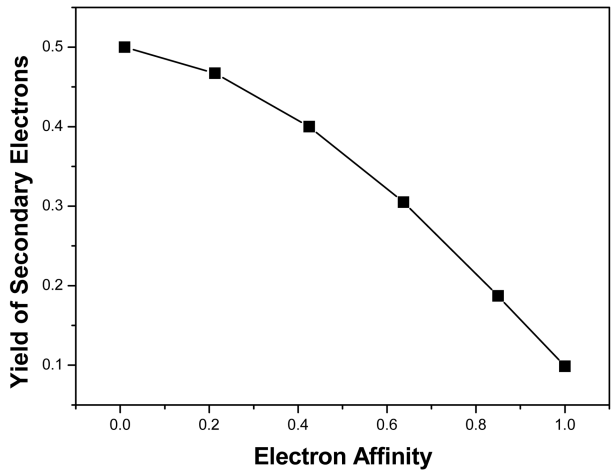

Fig. 24. The effect of electron affinity on the yield of secondary electrons via Auger neutralization reaction of Xe^+ ion with MgO. For this calculation, the band gap was assumed to be 4.8eV.

The effect of electron affinity on the yield of secondary electron emission for the Auger neutralization of Xe ions with MgO is shown in Fig. 24.[52] As noted from the figure, the yield increases significantly as the affinity decreases. This is mainly due to the fact that the fraction of electrons excited to the conduction band energy levels is decreased as the electron affinity decreases. Thus, it would be beneficial to have smaller electron affinity or negative affinity to obtain a higher yield. No experimental results related to this have been reported to date.

3) Effects of defect type and concentration in MgO

Impurities, dopants, or defects within MgO can have a significant influence on the yield of secondary electron emission by affecting the escape probability function and the energy band structure of MgO. Since MgO is a material dominantly having an ionic bonding characteristic, the impurities, dopants, or defects have effective charges. Therefore, these disorders can trap or scatter free current carriers such as electrons excited by the Auger neutralization reaction. The higher the density of such disorders, the higher the probability of trapping or scattering the excited electrons. For example, F^+-type centers can trap an electron by electrostatic attractive force, thereby decreasing the population density of excited electrons. This in turn that will reduce the yield of secondary electron emission. In addition, the scattering reaction may reduce the energy of some excited electrons below the vacuum level. This should decrease the density of electrons excited above the vacuum energy level and will also reduce the yield.

Using several escape probability curves proposed by Hagstrum,[51] and shown in Fig. 25, the effect of the escape probability on the yield of secondary electron emission was examined.[52] Curve 3 represents MgO with high purity and

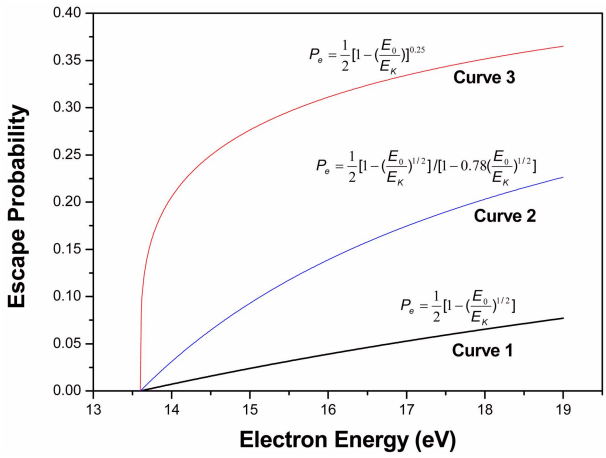

Fig. 25. Several escape probability curves proposed by Hagstrum [ ].

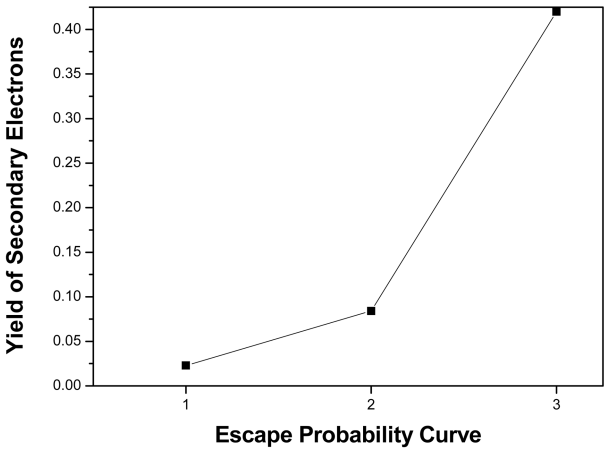

Fig. 26. Effect of escape probability on the yield of secondary electron emission.

low defect concentration and curve 1 is MgO with low purity and high defect concentration. As expected, the material with high escape probability (curve 3) shows a higher yield of secondary electron emission (Fig. 26). With increased impurities and defects, the yield can be decreased dramatically, indicating the MgO film produced by the e-beam evaporation process must have better crystallinity and high purity in order to lend an enhanced yield of secondary electrons.

Finally, disorders such as impurities, dopants, and defects in MgO create energy levels within the band gap. For example, the F-type centers are located roughly ~3 eV above the top of the valence band and contain one or two electrons. The electrons trapped in those energy levels may be excited above the vacuum level with less energy than the electrons in the valence band. The electrons trapped at those defect levels, therefore, may be able to contribute to secondary emission.

With the defects, there are four possible Auger neutralization reactions that may occur with Ne^+ ions when MgO has a F-type center, as shown in Fig. 27. According to the time-

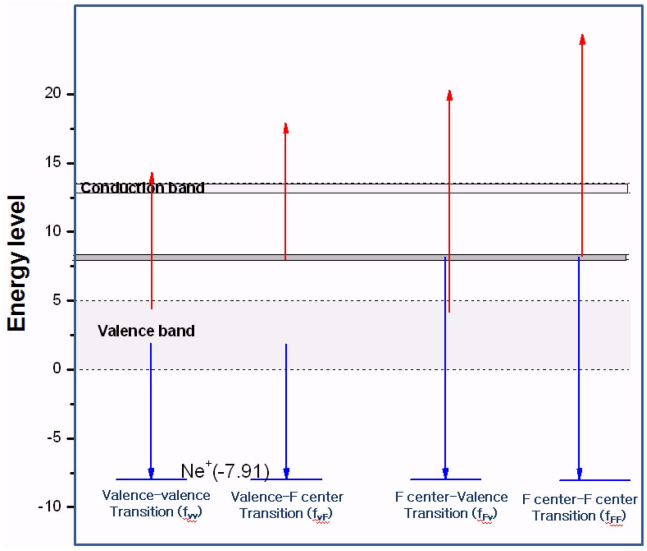

Fig. 27. Reaction types of Ne^+ ions approaching MgO with a defect level within band gap.

dependant perturbation theory, the probability of transition of electrons from MgO to approaching ions is proportional to the density of state. The probability of such electrons at trapped levels should be proportional to their mole fraction, as shown in following equation:

$$\gamma_i = N_v^2\gamma_{vv} + N_vN_F(\gamma_{vF} + \gamma_{Fv}) + N_F^2\gamma_{FF} \quad eqn.\ 18)$$

where N_v and N_F is the mole fraction of electrons at the valence band and at a F-type center, respectively. In a typical case, N_F is far less than 1,000 ppm ($N_F = 0.001$), and it can be seen from eqn. 18) that the contribution from the electrons trapped at defect levels to the emission of secondary electrons would be negligible. Therefore, it would be desirable to have high quality MgO with a low defect concentration in order to achieve improved secondary electron emission yield.

3. SUMMARY

We have reviewed the basic physics involved in the emission of secondary electrons from MgO during glow discharge of ac-PDPs. Emphasis was placed on the basic physics of the process, as better understanding of the electron emission process is the critical for enhancing the performance of ac-PDPs in terms of luminance efficacy, firing voltages, and addressing speed.

This paper reviewed intrinsic properties of MgO and extrinsic defects pertinent to the emission of electrons. The present review shows that MgO has physical properties that make it an ideal material for a protection and electron emission material under a glow discharge atmosphere. Based on the Hagstrum model, major parameters that may affect the yield of secondary electron emission were extracted. The parameters are type of discharge gas, band gap energy and electron affinity of MgO, and escape probability. The theoretical models show that secondary electron emission from the Auger neutralization reaction of Xe^+ with MgO is not feasible. One possible way to increase the yield from Xe^+ ions is to reduce the band gap energy of MgO. The escape probability of excited electrons was discussed in terms of scattering and trapping by defects formed in MgO. The results indicate that a high crystallinity and low impurity MgO thin film is needed for enhanced emission of secondary electron. Although in recent years progress has been made in the understanding of the electron emission mechanisms from MgO used for ac-PDPs, further systematic studies must be conducted to reduce the firing voltage and statistical delay of the addressing discharge, and to enhance the luminance efficiency of ac-PDPs.

ACKNOWLEDGEMENT

This work has been financially supported by the 21C Frontier Research Program through the Advanced Display Research Center and Hongik University. Authors would like appreciate their financial supports.

REFERENCES

1. R. H. Wilson, *"A capacitively coupled bistable gas discharge cell for computer controlled display,"* Univ. Illinois, Urbana-Champaign, Coordinated Sci. Lab. Rep. R-303 (1996).
2. D. L. Bitzer, H. G. Slottow, and R. H. Wilson, *U.S. Patent* # 3, 559, 190 (1971).
3. W. Siemens, *Poggendorff's Ann. Phys. Chem.* **102**, 66 (1857).
4. H. Uchiike, N. Nakayama, and M. Ohsawa, *Proc. Int. Electron Devices Meeting*, p. 191, Washington D.C. (1973).
5. H. S. Uhm, E. H. Choi and G. S. Cho, *Appl. Phys. Lett.* **78**, 592 (2001).
6. R. Ganter, Th. Callergari, L. C. Pitchford, and J. P. Boeuf, *Appl. Surf. Sci.* **192**, 299 (2002).
7. K. Yoshikawa, Y. Kanazawa, M. Wakitani, T. Shinoda, and O. Ohtsuka, *Japan Display Int. Display Res. Conf.*, p. 605, Hiroshima, Japan (1992).
8. M. Amatsuchi, A. Hirota, H. Lin, T. Naoi, E. Otani, H. Taniguchi, and K. Amemiya, *IDW'05 Tech. Digest*, p. 435 (2005).
9. T. Shiga, T. Mori, A. Saito, and S. Mikoshiba, *SID'05 Tech. Digest*, p. 1248 (2005).
10. L. F. Weber, *US Patent* # 6, 184, 848 (2001).
11. H. Tonlner, *IDW'04 Tech. Digest*, p. 921 (2004).
12. V. P. Nagorny, V. N. Khudik, and A. A. Shvydky, *IEEE Trans. Plasma Sci.* **34**, 343 (2006).
13. Q. Yan, N. Kosugi, Y. Oe, H. Tachibana, and L. F. Weber,

IDW'06 Tech. Digest, p. 359 (2006).
14. T. Sakashita, T. Shiga, and S. Mikoshiba, *IDW'06 Tech. Digest*, p. 1143 (2006).
15. H. S. Uhm, N. Yoo and E. H. Choi, *Phys. Plasmas* **14**, 043501 (2007).
16. L. Malter, *Phys. Rev. B* **50**, 48 (1936).
17. J. Kramer, *Der Metallische Zustand*, Vandenhoeck u. Ruprecht, Goettingen (1950).
18. P. A. Redhead, *J. Vac. Sci. Technol. A* **16**, 1394 (1998).
19. A. Einstein, *Annalen der Physik* **17**, 132 (1905).
20. C. Lushchik, A. Lushchik, T. Kyarner, M. Kirm, and S. Dolgov, *Russ. Phys. J.* **43**, 171 (2000).
21. Y. Chen, E. Montesa, J. L. Boldu and M. M. Abraham, *Phys. Rev. B* **24**, 5 (1981).
22. V. M. Orera and Y. Chen, *Phys. Rev. B* **36**, 5576 (1987).
23. G. H. Rosenblatt, R. W. Rowe, G. P. Williams, Jr., R. T. Williams, and Y. Chen, *Phys. Rev. B* **39**, 10309 (1989)
24. B. T. Jeffries, R. Gonzalez, Y. Chen, and G. P. Summers, *Phys. Rev. B* **25**, 2077 (1982)
25. M. A. Monge, R. Gonzalez, J. E. Munoz Santiuste, R. Pareja, Y. Chen, E. A. Kotomin, and A. I. Popov, *Nucl. Instrum. Methods Phys. Res. Sect. B* **166-167**, 220 (2000).
26. D. Sempolinski, W. D. Kingery, and H. L. Tuller, *J. Am. Ceram. Soc.* **63**, 669 (1980).
27. J. Fontanella, C. Andeen, and D. Schuele, *Appl. Phys. Lett.* **45**, 2852 (1974).
28. K. Kanaya, S. Ono, and F. Ishigaki, *J. Phys. D* **11**, 2425 (1978).
29. J. Portiera, G. Campeta, C. W. Kwona, J. Etourneaua, M. A. Subramanianb, *Int. J. Inorg. Mater.* **3**, 1091 (2001).
30. R. C. Whited, C. J. Flaten, and W. C. Walker, *Solid State Commun*. **13**, 1903 (1973).
31. B. Ulrici, W. Ulrici, and N. N. Kovalev, *Sov. Phys. Sol. St.* **17**, 2305 (1975).
32. M. O. Aboelfotoh and J. A. Lorenzen, *J. Appl. Phys.* **48**, 4754 (1977).
33. V. I. Avdeev and G. M. Zhidomirov, *J. Struct. Chem.* **44**, 918 (2003).
34. K. Y. Tsou and E. B. Hensley, *J. Appl. Phys.* **45**, 47 (1979).
35. J. Yamashita, *Phys. Rev. B* **111**, 733 (1958).
36. J. R. Stevenson and E. B. Hensley, *J. Appl. Phys.* **32**, 166 (1961).
37. N. D. Lang and W. Kohn, *Phys. Rev. B* **3**, 1215 (1971).
38. P. Riccardi, M. Ishimoto, P. Barone, and R. A. Baragiola, *Surf. Sci.* **571**, L305 (2004).
39. F. J. Himpsel, J. A. Knapp, J.A. VanVechten, and D. E. Eastman, *Phys. Rev. B* **20**, 624 (1979).
40. Y.-M Chiang, D. B. Birnie III, and W. D. Kingery, *Physical Ceramics*, p. 109, John Wiley & Sons, New York (1997).
41. O. Kubaschewski and C. B. Alcock, *Metallurgical Thermochemistry, International Series on Materials Science and Technology*, 5th ed., p. 292, Pergamon Press, Oxford (1979).
42. B. Henderson and J. E. Wertz, *Defects in the Alkaline Earth Oxides*, p. 4, Taylor & Francis LTD, London (1977).
43. Y.-M Chiang, D. B. Birnie III, and W. D. Kingery, *Physical Ceramics*, p. 129, John Wiley & Sons, New York (1997).
44. G. P. Summers, T. M. Wilson, B. T. Jeffries, H. T. Tohver, Y. Chen and M. M. Abraham, *Phys. Rev. B* **27**, 1283 (1983).
45. R. F. Pierret, *Semiconductor Fundamental*, 2nd ed., p. 33, Addison-Wesley, Reading, MA (1989).
46. B. Henderson and J. E. Wertz, *Defects in the Alkaline Earth Oxides*, p. 5, Taylor & Francis LTD, London (1977).
47. Y.-M Chiang, D. B. Birnie III, and W. D. Kingery, *Physical Ceramics*, p. 158, John Wiley & Sons, New York (1997).
48. G. Pacchioni and P. Pescarmona, *Surf. Sci.* **412-413**, 657 (1998).
49. J. Kramer, W. Ernst, C. Tegenkamp, and H. Hfnuer, *Surf. Sci.* **517**, 87 (2002).
50. H. Ebel, R. Svagera, and M. F. Ebel, *Adv. X-Ray Anal.* **43**, 519 (2000).
51. H. D. Hagstrum, *Phys. Rev. B* **122**, 83 (1961).
52. To be published
53. Y. Motoyama, H. Matsuzaki, and H. Murakami, *IEEE Trans. Electron Devices* **48**, 1568 (2001).
54. G. Oversluizen, T. Dekker, M. F. Gillies, and S. T. de Zwart, *J. Soc. Inf. Display* **12**, 51 (2004).